Image Reconstruction from Scattered Radon Data by Weighted Positive Definite Kernel Functions

S. De Marchi · A. Iske · G. Santin

December 11, 2017

Abstract We propose a novel kernel-based method for image reconstruction from scattered Radon data. To this end, we employ generalized Hermite-Birkhoff interpolation by positive definite kernel functions. For radial kernels, however, a straightforward application of the generalized Hermite-Birkhoff interpolation method fails to work, as we prove in this paper. To obtain a well-posed reconstruction scheme for scattered Radon data, we introduce a new class of *weighted* positive definite kernels, which are symmetric but not radially symmetric. By our construction, the resulting weighted kernels are combinations of radial positive definite kernels and positive weight functions. This yields very flexible image reconstruction methods, which work for arbitrary distributions of Radon lines. We develop suitable representations for the weighted basis functions and the symmetric positive definite kernel matrices that are resulting from the proposed reconstruction scheme. For the relevant special case, where Gaussian radial kernels are combined with Gaussian weights, explicit formulae for the weighted Gaussian basis functions and the kernel matrices are given. Supporting numerical examples are finally presented.

Keywords Image reconstruction · kernel-based approximation · generalized Hermite-Birkhoff interpolation · Radon transform · positive definite kernels

Stefano De Marchi
Department of Mathematics, University of Padua, Italy
E-mail: demarchi@math.unipd.it

Armin Iske
Department of Mathematics, University of Hamburg, Germany
E-mail: iske@math.uni-hamburg.de

Gabriele Santin
Institute of Applied Analysis and Numerical Simulation, University of Stuttgart, Germany
E-mail: gabriele.santin@mathematik.uni-stuttgart.de

1 Introduction

Computed Axial Tomography (CAT or CT) is a powerful technique to generate images from measurements of X-ray scans. One X-ray scan typically consists of several million of data samples, each of which corresponds to an X-ray beam passing through the computational domain, travelling from an emitter to a detector. The sensors of the operational CT scanner (positioned at the emitter and at the detector) then measures, for each X-ray beam, the loss of energy, resulting from the X-ray beam passing through the medium. The loss of energy reflects the ability of the medium to absorb energy, and so it depends on its specific structure and material properties. The amount of absorption can be described as a function of the computational domain Ω, termed *attenuation coefficient function*, $f : \Omega \to [0, \infty)$.

Medical imaging is only one relevant application for CT, where the primary goal is to reconstruct the unknown attenuation coefficient function f from given X-ray scans in order to generate clinically useful medical images. Other relevant applications are e.g. non-destructive evaluations of materials. In either case, robust numerical algorithms are required to reconstruct characteristic features of images at sufficiently high accuracy, on the one hand, and at sufficiently small computational costs, on the other hand. For details concerning the acquisition of X-ray scans, their underlying mathematical models, and standard computational methods for medical image reconstruction, we refer to the textbook [5] of Feeman.

To describe the mathematical problem of image reconstruction from X-ray scans, we regard the *Radon transform* $\mathcal{R}f$ of $f \in \mathrm{L}^1(\mathbb{R}^2)$, defined as

$$\mathcal{R}f(t,\theta) = \int_{\mathbb{R}} f(t\cos\theta - s\sin\theta, t\sin\theta + s\cos\theta)\,\mathrm{d}s \tag{1}$$

for $(t,\theta) \in \mathbb{R} \times [0,\pi)$. Note that for any $f \in \mathrm{L}^1(\mathbb{R}^2)$ the stability estimate

$$\|\mathcal{R}f(\cdot,\theta)\|_{\mathrm{L}^1(\mathbb{R})} \le \|f\|_{\mathrm{L}^1(\mathbb{R}^2)} \tag{2}$$

holds uniformly with respect to $\theta \in [0,\pi)$, and so we have $\mathcal{R}f \in \mathrm{L}^1(\mathbb{R} \times [0,\pi))$ for all $f \in \mathrm{L}^1(\mathbb{R}^2)$. Therefore, the Radon transform $\mathcal{R} : \mathrm{L}^1(\mathbb{R}^2) \to \mathrm{L}^1(\mathbb{R}\times[0,\pi))$ in (1) is well-defined on $\mathrm{L}^1(\mathbb{R}^2)$.

We remark that the Radon transform $\mathcal{R}f(t,\theta)$ gives, for any fixed pair $(t,\theta) \in \mathbb{R} \times [0,\pi)$, a line integral for f over a specific straight line $\ell \equiv \ell_{t,\theta}$. In order to see this, let $\ell_{t,\theta} \subset \mathbb{R}^2$ denote the unique straight line, which is perpendicular to the unit vector $\mathbf{n}_\theta = (\cos\theta, \sin\theta)$ and which passes through the point $p = (t\cos\theta, t\sin\theta) = t\mathbf{n}_\theta$. In this case, $\ell_{t,\theta}$ can be parameterized as

$$\mathbf{x}(s) = (x_1(s), x_2(s)) = (t\cos\theta - s\sin\theta, t\sin\theta + s\cos\theta) \qquad \text{for } s \in \mathbb{R}. \tag{3}$$

By this specific choice for a parameterization of $\ell_{t,\theta}$ in (3), we see that the line integral of f over $\ell_{t,\theta}$ coincides with the Radon transform $\mathcal{R}f(t,\theta)$ in (1), i.e.,

$$\int_{\ell_{t,\theta}} f(\mathbf{x})\,\mathrm{d}\mathbf{x} := \int_{\mathbb{R}} f(\mathbf{x}(s))\,\mathrm{d}s = \mathcal{R}f(t,\theta) \qquad \text{for } (t,\theta) \in \mathbb{R} \times [0,\pi).$$

On the other hand, any straight line ℓ in the plane can be described by a unique pair (t, θ) of a radial parameter $t \in \mathbb{R}$ and an angular parameter $\theta \in [0, \pi)$ satisfying $\ell \equiv \ell_{t,\theta}$. In this way, the Radon transform $\mathcal{R}f$ of f is a linear integral transformation, which maps any bivariate function $f \in \mathrm{L}^1(\mathbb{R}^2)$ (in Cartesian coordinates) onto a bivariate function $\mathcal{R}f \in \mathrm{L}^1(\mathbb{R} \times [0, \pi))$ (in polar coordinates), where the image $\mathcal{R}f$ contains all line integrals of f over the set of straight lines in the plane.

Due the seminal work [14] of Johann Radon, any $f \in \mathrm{L}^1(\mathbb{R}^2) \cap \mathscr{C}(\mathbb{R}^2)$ can be reconstructed from its Radon transform $\mathcal{R}f$. The inversion of the Radon transform is given by the *filtered back projection* (FBP) formula (see [5, Chapter 6]),

$$f(\mathbf{x}) = \frac{1}{2}\mathcal{B}\left\{\mathcal{F}^{-1}\left[|S|\mathcal{F}(\mathcal{R}f)(S,\theta)\right]\right\}(\mathbf{x}), \tag{4}$$

where $\mathcal{F}$ is, for any fixed angle θ, the *univariate* Fourier transform w.r.t. the radial variable t, and so is $\mathcal{F}^{-1}$ the univariate inverse Fourier transform w.r.t. the frequency variable S. Moreover, the *back projection* $\mathcal{B}$ is, for any function $h \equiv h(t, \theta)$ (in polar coordinates), given by the average

$$\mathcal{B}h(\mathbf{x}) = \frac{1}{\pi}\int_0^\pi h(x_1 \cos\theta + x_2 \sin\theta, \theta)\,\mathrm{d}\theta$$

of $h(t, \theta)$ over the angular variable θ, where we let

$$t = x_1 \cos\theta + x_2 \sin\theta = \mathbf{x} \cdot \mathbf{n}_\theta$$

according to the one-to-one relation between the polar coordinates (t, θ) and the Cartesian coordinates $\mathbf{x} = (x_1, x_2)$, as described above along with the parameterization of the lines $\ell_{t,\theta}$ in (3). For basic details concerning the derivation of the filtered back projection formula, we refer to [5]. We remark that the well-posedness of the Radon inverse problem has already been studied in [9]. For a more comprehensive mathematical treatment of the Radon transform and its inversion, we refer to the textbooks [8,13].

In practical application scenarios, however, only a *finite* set of Radon data,

$$\mathcal{R}_\mathcal{L}(f) = \{\mathcal{R}f(t_k, \theta_k)\}_{k=1}^m, \tag{5}$$

given as integrals of f over a finite set of m pairwise distinct lines,

$$\mathcal{L} = \{\ell_{t_k,\theta_k} : (t_k, \theta_k) \in \mathbb{R} \times [0, \infty) \text{ for } k = 1, \ldots, m\},$$

is available. In this case, an approximate reconstruction of f from Radon data $\mathcal{R}_\mathcal{L}f$ is sought. In standard techniques of medical imaging, the reconstruction of f is accomplished by using a suitable discretization of the FBP in (4). For this class of Fourier-based reconstruction methods, the discrete lines in $\mathcal{L}$, over which the line integrals of f are known, are usually required to be regularly spaced in the plane, e.g. by assuming *parallel beam geometry* or *fan beam geometry* (see [5] for particular assumptions on the geometry of $\mathcal{L}$).

In many realistic scenarios of data acquisition, however, we may face a limited range of angles (e.g. in mammography), or a limited dosage of X-ray expositions, so that the Radon data are partly corrupt or incomplete. In such relevant cases, the Radon data in (5) are *scattered*, i.e., the distribution of lines in $\mathcal{L}$ is essentially *not* regular but scattered, in which case standard Fourier methods, such as the Fourier-based FBP discretization in (4), do no longer apply. This requires more flexible approximation methods which work for arbitrary geometries of (scattered) Radon lines $\mathcal{L}$.

To approximate f from *scattered* Radon data $\mathcal{R}_{\mathcal{L}} f$, *algebraic reconstruction techniques* (ART) [6] can be applied. The concept of ART is essentially different from that of Fourier-based reconstructions: in the setting of ART one fixes a set $\{g_j\}_{j=1}^n$ of basis functions beforehand to solve the reconstruction problem

$$\mathcal{R}_{\mathcal{L}}(g) = \mathcal{R}_{\mathcal{L}}(f) \tag{6}$$

by using a linear combination

$$g = \sum_{j=1}^{n} c_j g_j$$

of the basis functions. According to our problem formulation at the outset of this introduction, we require $g_j \in \mathrm{L}^1(\mathbb{R}^2)$, for all $1 \leq j \leq n$, so that the Radon transform $\mathcal{R}g_j$, as in (1), is for any basis function g_j well-defined. This then amounts to solving the linear system

$$Ac = b \tag{7}$$

for the unknown coefficients $c = (c_1, \ldots, c_n)^T \in \mathbb{R}^n$ of g, where the $m \times n$ matrix A has the form

$$A = (\mathcal{R}g_j(t_k, \theta_k))_{k=1,\ldots,m;j=1,\ldots,n} \in \mathbb{R}^{m \times n} \tag{8}$$

and where $b = (b_1, \ldots, b_m)^T \in \mathbb{R}^m$ is given by the m Radon observations $b_k = \mathcal{R}f(t_k, \theta_k)$, for $k = 1, \ldots, m$. But for the well-posedness of the resulting ART reconstruction scheme, we require that all matrix entries $a_{kj} = g_j(t_k, \theta_k)$ of A in (8) and all entries $b_k = \mathcal{R}f(t_k, \theta_k)$ are finite. We will be more specific on this assumption in the following discussion of this paper.

Unless the number m of Radon samples coincides with the number n of coefficients, the linear system in (7) is either overdetermined, for $m > n$, or underdetermined, for $n > m$. In case of an overdetermined system, the classical method of *linear least squares approximation* [2] is applied to minimize the residual (Euclidean) norm $\|Ac - b\|$, whereas for an underdetermined system the iterative method of Kaczmarz [5, Section 9.3] is a standard tool to compute an approximate solution c satisfying $Ac \approx b$. We remark that in either case the linear system in (7) is not guaranteed to have a unique solution, not even when $m = n$. In fact, the latter is due to the *Mairhuber-Curtis theorem* [17, Section 2.1] from multivariate approximation theory.

A first kernel-based approach for scattered data interpolation from Radon data was developed in [1]. The resulting kernel method in [1] transfers the reconstruction problem (6) into one for suitable projective spaces, on which positive definite zonal functions are utilized to accomplish the recovery step. We remark that the straightforward approach taken in this paper is essentially different from that in [1], although [1] relies on positive definite kernels, too.

In previous work [4], we considered using radially symmetric kernels in combination with regularizations of the Radon transform. The approach taken in [4], however, leads to linear systems (7) with unsymmetric matrices A. In this paper, we propose a well-posed kernel-based reconstruction method, whose resulting kernel matrices $A \in \mathbb{R}^{n\times n}$ are symmetric and positive definite. Our proposed reconstruction scheme relies on the theory of kernel-based multivariate interpolation from generalized Hermite-Birkhoff data [11]. We adapt this particular interpolation scheme to the special case of image reconstruction from scattered Radon data. In this case, the basis functions in $\{g_j\}_{j=1}^n$ must essentially depend on the given Radon functionals $\mathcal{R}_{\mathcal{L}}$. We show that an uncustomized application of generalized Hermite-Birkhoff reconstruction fails to work for radially symmetric kernels. To guarantee the well-posedness of the reconstruction scheme, particularly to obtain well-defined entries in A, we develop a general concept for the construction of *weighted* positive definite kernels. The resulting kernels are symmetric but not radially symmetric. We give examples for suitable pairs of radial weights and radial positive definite functions. This yields a new class of flexible reconstruction schemes, which work for arbitrary distributions of scattered Radon lines.

The outline of this paper is as follows. In Section 2, we briefly review generalized Hermite-Birkhoff interpolation, where we show how to adapt this particular reconstruction method to scattered Radon data. In Section 3, we introduce weighted radial kernels, where we explain how they are used to obtain a well-posed reconstruction method. Moreover, we develop suitable representations for the resulting basis functions g_j and the matrix entries for A in (8). This is followed by a discussion concerning one special case, where standard Gaussian kernels are combined with Gaussian weights. For this prototypical case, covered in Section 4, we give explicit formulae for the resulting Gaussian basis functions g_j and the Gaussian matrix entries a_{kj}. For the purpose of illustration, numerical results are finally provided in Section 5.

2 Generalized Hermite-Birkhoff Interpolation

To solve the reconstruction problem (6), we consider applying Hermite-Birkhoff interpolation [11]. Let us first explain the general framework of Hermite-Birkhoff interpolation, before we apply Hermite-Birkhoff interpolation to the special case of reconstruction from scattered Radon data. According to the generic formulation of the Hermite-Birkhoff reconstruction problem, we first fix a linear function space $\mathcal{F}$. Moreover, we assume a finite set $\Lambda = \{\lambda_1, \ldots, \lambda_n\}$ of linearly independent linear functionals $\lambda_j : \mathcal{F} \to \mathbb{R}$ to be given, so that for

any $f \in \mathcal{F}$, the action of any functional $\lambda_j \in \Lambda$ on f is well-defined, for $1 \leq j \leq n$. This yields, for any $f \in \mathcal{F}$ a data vector of samples

$$f_\Lambda = (\lambda_1(f), \ldots, \lambda_n(f))^T \in \mathbb{R}^n.$$

Now the solution of the Hermite-Birkhoff reconstruction problem requires finding a function g satisfying the interpolation conditions $g_\Lambda = f_\Lambda$, i.e.,

$$\lambda_k(g) = \lambda_k(f) \qquad \text{for all } k = 1, \ldots, n. \tag{9}$$

To this end, a finite set $\{g_j\}_{j=1}^n$ of *suitable* linearly independent functions $g_j \in \mathcal{F}$ is selected. This gives the finite-dimensional linear reconstruction space

$$\mathcal{G} := \operatorname{span}\{g_1, \ldots, g_n\} \subset \mathcal{F}, \tag{10}$$

from which a solution $g \in \mathcal{G}$ of the Hermite-Birkhoff interpolation problem (9) is to be determined.

Note that the general framework of Hermite-Birkhoff interpolation can be applied to the reconstruction problem (6). In this particular case, the linear functionals $\lambda_k : \mathcal{F} \to \mathbb{R}$ are defined via the Radon functionals

$$\lambda_k(f) := \mathcal{R}_k f \equiv \mathcal{R} f(t_k, \theta_k) \qquad \text{for } k = 1, \ldots, n,$$

where we let $\mathcal{F} = \mathrm{L}^1(\mathbb{R}^2)$ according to our setup from the introduction.

By the interpolation conditions in (9), we obtain n linear equations,

$$\sum_{j=1}^{n} c_j \lambda_k(g_j) = \lambda_k(f) \qquad \text{for } k = 1, \ldots, n,$$

corresponding to the linear system in (7). By the choice of the Hermite-Birkhoff reconstruction space $\mathcal{G}$ in (10) the number of equations, n, matches the number of basis functions in $\{g_j\}_{j=1}^n$. In other words, the number of interpolation conditions coincides with the dimension of the reconstruction space $\mathcal{G}$. Therefore, we have $n = m$ by construction, and so the linear system in (7) is n-by-n, with a square matrix $A \in \mathbb{R}^{n \times n}$ in (8).

Now let us address the selection of *suitable* basis functions $g_j \in \mathcal{F}$. According to the general framework of the Hermite-Birkhoff interpolation scheme, we need to fix a *suitable* function $K : \mathbb{R}^2 \times \mathbb{R}^2 \to \mathbb{R}$, whose properties we explain in the following discussion. Then, the basis functions g_j in (10) are assumed to have the form

$$g_j(\mathbf{x}) = \lambda_j^{\mathbf{y}} K(\mathbf{x}, \mathbf{y}) \qquad \text{for } j = 1, \ldots, n, \tag{11}$$

where $\lambda_j^{\mathbf{y}} K(\mathbf{x}, \mathbf{y})$ denotes the action of the functional λ_j on K w.r.t. $\mathbf{y} \in \mathbb{R}^2$. Recall that $g_j \in \mathcal{F}$, which leads to the requirement $\lambda_j^{\mathbf{y}} K(\cdot, \mathbf{y}) \in \mathcal{F}$ for K.

Moreover we require K to be *symmetric*, i.e.,

$$K(\mathbf{x}, \mathbf{y}) = K(\mathbf{y}, \mathbf{x}) \quad \text{for all } \mathbf{x}, \mathbf{y} \in \mathbb{R}^2,$$

and *positive definite*. Rather than dwelling much on explaining positive definite functions, we remark that for the purposes of this paper it is sufficient to say that a continuous function $K \equiv K(\mathbf{x}, \mathbf{y})$ is symmetric and *positive definite*, iff the matrix

$$A_{K,\Lambda} = \left(\lambda_j^{\mathbf{x}} \lambda_k^{\mathbf{y}} K(\mathbf{x}, \mathbf{y})\right)_{1 \le j,k \le n} \in \mathbb{R}^{n \times n} \tag{12}$$

is symmetric positive definite for any set $\Lambda = \{\lambda_j\}_{j=1}^n$ of linearly independent functionals λ_j. For a more comprehensive account to the construction and characterization of positive definite functions, we refer the reader to [12,15]. We remark that positive definite functions K lead to Hilbert spaces $\mathcal{F}$ with reproducing kernel K. Therefore, we call K a positive definite *kernel* function. For a recent account to reproducing kernels in data science we refer to [7].

Before we make concrete examples for suitable (symmetric and positive definite) kernels K, the following remarks are in order.

Remark 1 For the special case of Lagrange interpolation, i.e., interpolation from point values, commonly used positive definite kernels K are *radially symmetric*, i.e., K has the form

$$K_\phi(\mathbf{x}, \mathbf{y}) = \phi(\|\mathbf{x} - \mathbf{y}\|^2) \qquad \text{for } \mathbf{x}, \mathbf{y} \in \mathbb{R}^2,$$

for a continuous function $\phi : [0, \infty) \to \mathbb{R}$ of the Euclidean norm $\|\cdot\|$ on $\mathbb{R}^2$. □

Among the most prominent examples for radially symmetric kernels are the *Gaussians*

$$\phi_\alpha(\|\mathbf{x}\|^2) = \mathrm{e}^{-\alpha\|\mathbf{x}\|^2} \quad \text{for } \mathbf{x} \in \mathbb{R}^2$$

that are for any $\alpha > 0$ positive definite, i.e.,

$$K(\mathbf{x}, \mathbf{y}) = \exp(-\alpha\|\mathbf{x} - \mathbf{y}\|^2)$$

is positive definite. Other popular examples are the *inverse multiquadrics*,

$$\phi_\alpha(\|\mathbf{x}\|^2) = \frac{1}{(1 + \alpha\|\mathbf{x}\|^2)^\beta} \quad \text{for } \mathbf{x} \in \mathbb{R}^2 \text{ and } \alpha > 0,$$

which are positive definite for any $\beta \in (0, 1)$.

Remark 2 For the special case of Radon data, however, the selection of a suitable positive definite kernel requires particular care. To further explain this, note that the reconstruction method can only work, if the basis functions g_j in (11) are well-defined, and, moreover, all entries in matrix A in (12) are well-defined. To guarantee well-defined basis functions g_j, we merely require

$$\phi(\|\mathbf{x} - \cdot\|^2) \in \mathrm{L}^1(\mathbb{R}^2) \qquad \text{for all } \mathbf{x} \in \mathbb{R}^2,$$

i.e., $\phi(\|\cdot\|^2) \in \mathrm{L}^1(\mathbb{R}^2)$, in which case the stability estimate (2) holds for $g_j(\mathbf{x}) = \mathcal{R}_j^{\mathbf{y}} K_\phi(\mathbf{x}, \mathbf{y})$. Note that this property is satisfied by the Gaussians, but not by the inverse multiquadrics, and so one could argue this is only a minor problem. The other point concerning well-defined entries in A is, indeed, more severe. □

To further explain this problem, let us provide the following negative result.

Proposition 1 *Let $\phi(\|\cdot\|^2) \in \mathrm{L}^1(\mathbb{R}^2)$ be continuous and positive definite, and let $\ell \subset \mathbb{R}^2$ be a straight line in the plane. Then the double line integral*

$$\int_\ell \int_\ell \phi(\|\mathbf{x}-\mathbf{y}\|^2)\,\mathrm{d}\mathbf{y}\,\mathrm{d}\mathbf{x} \tag{13}$$

is divergent.

Proof Note that the positive definite function $\phi(\|\cdot\|^2)$ attains its unique maximum at zero, where $\phi(0) > 0$, i.e., $\phi \not\equiv 0$. Moreover, note that the line integral

$$I(\mathbf{x}) = \int_\ell \phi(\|\mathbf{x}-\mathbf{y}\|^2)\,\mathrm{d}\mathbf{y} \qquad \text{for } \mathbf{x} \in \ell$$

is finite and constant on ℓ, where $I(\mathbf{x}) \equiv I(\mathbf{0}) \neq 0$, since ϕ is positive definite. Therefore, the double integral in (13) cannot be finite. □

In conclusion, the above proposition states that for any radially symmetric kernel $K_\phi(\mathbf{x},\mathbf{y}) = \phi(\|\mathbf{x}-\mathbf{y}\|^2)$, the diagonal entries of the matrix $A_{K,\Lambda}$ in (12) are (for the case of Radon functionals) *singular*, as they are given by the double line integrals

$$\mathcal{R}_k^{\mathbf{x}}\mathcal{R}_k^{\mathbf{y}}\phi(\|\mathbf{x}-\mathbf{y}\|^2) = \int_{\ell_k}\int_{\ell_k} \phi(\|\mathbf{x}-\mathbf{y}\|^2)\,\mathrm{d}\mathbf{y}\,\mathrm{d}\mathbf{x}$$

for straight lines $\ell_k \subset \mathbb{R}^2$, $1 \le k \le n$. In this case, an uncustomized application of generalized Hermite-Birkhoff interpolation is therefore doomed to fail.

3 Weighted Positive Definite Kernels

In standard applications of kernel-based approximation, the utilized kernel

$$K_\phi(\mathbf{x},\mathbf{y}) = \phi(\|\mathbf{x}-\mathbf{y}\|^2) \qquad \text{for } \phi \in \mathbf{PD}(\mathbb{R}^d) \tag{14}$$

is radially symmetric (i.e., invariant under rotations of the coordinate system) and shift-invariant (i.e., invariant under translations of the coordinates).

Now we prefer to work with *weighted* kernels of the form

$$K_{\phi,w}(\mathbf{x},\mathbf{y}) = \phi(\|\mathbf{x}-\mathbf{y}\|^2)w(\|\mathbf{x}\|^2)w(\|\mathbf{y}\|^2) \qquad \text{for } \mathbf{x},\mathbf{y} \in \mathbb{R}^2, \tag{15}$$

where $w : [0,\infty) \to (0,\infty)$ is a *weight function*. Note that for $w \equiv 1$ we have $K_{\phi,1} \equiv K_\phi$, and so the set of weighted kernels $K_{\phi,w}$ in (15) is an extension to the set of kernels K_ϕ in (14). Moreover, note that any weighted kernel $K_{\phi,w}$ of the form (15) is symmetric, but (for the case of non-constant weights w) neither radially symmetric nor shift-invariant, unlike K_ϕ in (14).

We remark that the choice of $K_{\phi,w}$ in (15) will, for *suitable* combinations of kernels ϕ and weights w, guarantee both well-defined basis functions g_j in (11) and well-defined matrix entries in (12). This, in fact, is the purpose of

our proposed extension from the kernels K_ϕ in (14) to the weighted kernels $K_{\phi,w}$ in (15). The required conditions on ϕ and w will be detailed in Theorem 1 and in Proposition 4.

Next we show that any weighted kernel $K_{\phi,w}$ in (15) is positive definite w.r.t. the *Schwartz space*

$$\mathcal{S} := \left\{\gamma \in \mathscr{C}^\infty(\mathbb{R}^d;\mathbb{R}) : D^p\gamma(\mathbf{x})\mathbf{x}^q \to 0 \text{ for all } p,q \in \mathbb{N}_0^d\right\}$$

of all rapidly decaying $\mathscr{C}^\infty$ functions [10,11].

Definition 1 A continuous and symmetric function $K : \mathbb{R}^d \times \mathbb{R}^d \to \mathbb{R}$ is said to be `positive definite` on $\mathcal{S}$, $K \in \mathbf{PD}(\mathcal{S})$, iff the double integral

$$\int_{\mathbb{R}^d}\int_{\mathbb{R}^d} K(\mathbf{x},\mathbf{y})\gamma(\mathbf{x})\gamma(\mathbf{y})\,\mathrm{d}\mathbf{x}\,\mathrm{d}\mathbf{y} \tag{16}$$

is positive for all $\gamma \in \mathcal{S}\setminus\{0\}$. □

The following observation will be important for our subsequent analysis.

Proposition 2 *Let $K \equiv K_\Phi : \mathbb{R}^d \times \mathbb{R}^d \to \mathbb{R}$ be of the form*

$$K_\Phi(\mathbf{x},\mathbf{y}) = \Phi(\mathbf{x}-\mathbf{y}) \qquad \textit{for } \mathbf{x},\mathbf{y} \in \mathbb{R}^d, \tag{17}$$

for an even function $\Phi \in \mathrm{L}^1(\mathbb{R}^d,\mathbb{R}) \cap \mathscr{C}(\mathbb{R}^d,\mathbb{R})$. If K_Φ is positive definite on $\mathcal{S}$, $K_\Phi \in \mathbf{PD}(\mathcal{S})$, then the Fourier transform

$$\hat{\Phi}(\mathbf{z}) = \int_{\mathbb{R}^d} \Phi(\mathbf{x})\,\mathrm{e}^{-\mathrm{i}\mathbf{x}^T\mathbf{z}}\,\mathrm{d}\mathbf{x} \qquad \textit{for } \mathbf{z} \in \mathbb{R}^d$$

is positive on $\mathbb{R}^d$, i.e., $\hat{\Phi}(\mathbf{z}) > 0$ for all $\mathbf{z} \in \mathbb{R}^d$.

Proof By our assumptions on Φ, we can rely on the *Fourier inversion theorem*,

$$\Phi(\mathbf{x}-\mathbf{y}) = (2\pi)^{-d}\int_{\mathbb{R}^d} \hat{\Phi}(\mathbf{z})\mathrm{e}^{\mathrm{i}(\mathbf{x}-\mathbf{y})^T\mathbf{z}}\,\mathrm{d}\mathbf{z}\,,$$

so that, for any $\gamma \in \mathcal{S}$, we find the representation

$$\begin{aligned}\int_{\mathbb{R}^d}\int_{\mathbb{R}^d} K_\Phi(\mathbf{x},\mathbf{y})\gamma(\mathbf{x})\gamma(\mathbf{y})\,\mathrm{d}\mathbf{x}\,\mathrm{d}\mathbf{y} &= \int_{\mathbb{R}^d}\int_{\mathbb{R}^d} \Phi(\mathbf{x}-\mathbf{y})\gamma(\mathbf{x})\gamma(\mathbf{y})\,\mathrm{d}\mathbf{x}\,\mathrm{d}\mathbf{y}\\ &= (2\pi)^{-d}\int_{\mathbb{R}^d} \hat{\Phi}(\mathbf{z})\left(\int_{\mathbb{R}^d}\gamma(\mathbf{x})\mathrm{e}^{-\mathrm{i}\mathbf{x}^T\mathbf{z}}\,\mathrm{d}\mathbf{x}\right)^2\,\mathrm{d}\mathbf{z}\\ &= (2\pi)^{-d}\int_{\mathbb{R}^d} \hat{\Phi}(\mathbf{z})\,|\hat{\gamma}(\mathbf{z})|^2\,\mathrm{d}\mathbf{z}.\end{aligned}$$

From this we see that $\hat{\Phi}$ is positive on $\mathbb{R}^d$, since the double integral in (16) is assumed to be positive for all $\gamma \in \mathcal{S}\setminus\{0\}$. □

From now we will say that Φ in (17) is *positive definite* on $\mathcal{S}$, $\Phi \in \mathbf{PD}(\mathcal{S})$, iff $K_\Phi \in \mathbf{PD}(\mathcal{S})$. We can draw the following conclusion from Proposition 2.

Corollary 1 *Let $\Phi \in \mathrm{L}^1(\mathbb{R}^d,\mathbb{R}) \cap \mathscr{C}(\mathbb{R}^d,\mathbb{R})$ be even and positive definite on $\mathcal{S}$. Moreover, let $w : \mathbb{R}^d \to (0,\infty)$ be a continuous function of at most polynomial growth around infinity. Then, the function*

$$K_{\Phi,w}(\mathbf{x},\mathbf{y}) = \Phi(\mathbf{x}-\mathbf{y})w(\mathbf{x})w(\mathbf{y}) \qquad \text{for } \mathbf{x},\mathbf{y} \in \mathbb{R}^d$$

is symmetric and positive definite on $\mathcal{S}$.

Proof Like in the proof of Proposition 2, we can establish the representation

$$\begin{aligned}\int_{\mathbb{R}^d}\int_{\mathbb{R}^d} K_{\Phi,w}(\mathbf{x},\mathbf{y})\gamma(\mathbf{x})\gamma(\mathbf{y})\,\mathrm{d}\mathbf{x}\,\mathrm{d}\mathbf{y} &= \int_{\mathbb{R}^d}\int_{\mathbb{R}^d} \Phi(\mathbf{x}-\mathbf{y})w(\mathbf{x})\gamma(\mathbf{x})w(\mathbf{y})\gamma(\mathbf{y})\,\mathrm{d}\mathbf{x}\,\mathrm{d}\mathbf{y} \\ &= (2\pi)^{-d}\int_{\mathbb{R}^d} \hat{\Phi}(\mathbf{z})\,|\widehat{w\gamma}(\mathbf{z})|^2\,\mathrm{d}\mathbf{z}. \qquad (18)\end{aligned}$$

Recall $\hat{\Phi} > 0$ from Proposition 2. Moreover, since w is positive on $\mathbb{R}^d$, the integral in (18) is positive for all $\gamma \in \mathcal{S}\setminus\{0\}$, and so $K_{\Phi,w} \in \mathbf{PD}(\mathcal{S})$. □

We remark that any positive definite function K on $\mathcal{S}$, $K \in \mathbf{PD}(\mathcal{S})$, is also positive definite on $\mathbb{R}^d$, $K \in \mathbf{PD}(\mathbb{R}^d)$. In other words, $K \in \mathbf{PD}(\mathcal{S})$ generates, for any set $\mathbf{X} = \{\mathbf{x}_1,\ldots,\mathbf{x}_n\} \subset \mathbb{R}^d$ of pairwise distinct points, a symmetric positive definite *kernel matrix*

$$A_{K,\mathbf{X}} = (K(\mathbf{x}_j,\mathbf{x}_k))_{1\le j,k\le n} \in \mathbb{R}^{n\times n},$$

by point evaluations of $K(\mathbf{x},\mathbf{y})$ at $\mathbf{X}\times\mathbf{X}$, and so we have

$$\mathbf{PD}(\mathcal{S}) \subset \mathbf{PD}(\mathbb{R}^d).$$

As shown in [10,11], the above inclusion is a rather straightforward consequence from the celebrated Bochner theorem [3], several of whose variants were used to construct positive definite radial kernels — "radial basis functions" — for the purpose of multivariate approximation from Lagrange data [15].

In the situation of this paper, we wish to work with positive definite kernels $K \in \mathbf{PD}(\mathcal{S})$, all of whose kernel matrices

$$A_{K,\mathcal{L}} = \left(\mathcal{R}^{\mathbf{x}}_{\ell_j}\mathcal{R}^{\mathbf{y}}_{\ell_k}K(\mathbf{x},\mathbf{y})\right) \in \mathbb{R}^{n\times n}, \qquad (19)$$

generated by integrals along a set of pairwise distinct Radon lines,

$$\mathcal{L} = \{\ell_1,\ldots,\ell_n\} \subset \mathbb{R}^2\,,$$

are symmetric positive definite. We call such kernels K positive definite with respect to the Radon transform $\mathcal{R}$, or, in short, $K \in \mathbf{PD}(\mathcal{R})$. As shown in Proposition 1, the class $\mathbf{PD}(\mathcal{R})$ contains no radially symmetric function K.

Therefore, we use weighted positive definite kernels $K_{\phi,w}$ of the form (15). Now the well-posedness of the resulting reconstruction scheme follows from [11]. For the reader's convenience, we summarize our discussion as follows.

Theorem 1 *Let $K_\phi(\mathbf{x},\mathbf{y}) = \phi(\|\mathbf{x}-\mathbf{y}\|^2)$ be a positive definite function on $\mathcal{S}$, $K_\phi \in \mathbf{PD}(\mathcal{S})$, and let $w : [0,\infty) \to (0,\infty)$ be continuous and positive. Moreover, suppose*

$$(\phi w)(|\cdot|^2) \in \mathrm{L}^1([0,\infty),\mathbb{R}).$$

Then, $K_{\phi,w}$ in (15) is positive definite w.r.t. $\mathcal{R}$, i.e., $K_{\phi,w} \in \mathbf{PD}(\mathcal{R})$. □

In the remainder of this section, we develop for weighted kernels $K_{\phi,w}$ of the form (15) suitable representations for their associated basis functions

$$g_{t,\theta}(\mathbf{x}) = \mathcal{R}^{\mathbf{y}}_{\ell_{t,\theta}} K_{\phi,w}(\mathbf{x},\mathbf{y}) \qquad \text{for } \ell_{t,\theta} \in \mathcal{L} \tag{20}$$

and for their matrix entries

$$a_{kj} = \mathcal{R}^{\mathbf{x}}_{\ell_j} \mathcal{R}^{\mathbf{y}}_{\ell_k} K_{\phi,w}(\mathbf{x},\mathbf{y}) \qquad \text{for } \ell_j, \ell_k \in \mathcal{L}. \tag{21}$$

3.1 Representation of the Weighted Basis Functions

In this section, we compute suitable representations for the weighted basis functions $g_{t,\theta}$ in (20). For $K_{\phi,w}$ in (15), any $g_{t,\theta}$ in (20) can be written as

$$g_{t,\theta}(\mathbf{x}) = \mathcal{R}^{\mathbf{y}}_{t,\theta}\left[\phi(\|\mathbf{x}-\mathbf{y}\|^2) w(\|\mathbf{y}\|^2)\right] \cdot w(\|\mathbf{x}\|^2)\,, \tag{22}$$

where $\mathcal{R}_{t,\theta}$ is the Radon transform on line $\ell \equiv \ell_{t,\theta}$ for $(t,\theta) \in \mathbb{R} \times [0,\pi)$.

To compute $g_{t,\theta}(\mathbf{x}) = h_{t,\theta}(\mathbf{x}) \cdot w(\|\mathbf{x}\|^2)$, we represent its major part as

$$\begin{aligned}
h_{t,\theta}(\mathbf{x}) &= \mathcal{R}^{\mathbf{y}}_{t,\theta}\left[\phi(\|\mathbf{x}-\mathbf{y}\|^2) w(\|\mathbf{y}\|^2)\right] \\
&= \int_{\ell_{t,\theta}} \phi(\|\mathbf{x}-\mathbf{y}\|^2) w(\|\mathbf{y}\|^2)\,\mathrm{d}\mathbf{y} \\
&= \int_{\ell_{t,0}} \phi(\|\mathbf{x}-Q_\theta\mathbf{y}\|^2) w(\|Q_\theta\mathbf{y}\|^2)\,\mathrm{d}\mathbf{y} \\
&= \int_{\ell_{t,0}} \phi(\|Q_\theta^{-1}\mathbf{x}-\mathbf{y}\|^2) w(\|\mathbf{y}\|^2)\,\mathrm{d}\mathbf{y} \\
&= \int_{\ell_{t,0}} \phi(\|\mathbf{x}_\theta-\mathbf{y}\|^2) w(\|\mathbf{y}\|^2)\,\mathrm{d}\mathbf{y},
\end{aligned}$$

with the rotation matrix

$$Q_\theta = \begin{bmatrix} \cos(\theta) & -\sin(\theta) \\ \sin(\theta) & \cos(\theta) \end{bmatrix} = \left[\mathbf{n}_\theta | \mathbf{n}_\theta^\perp\right] \qquad \text{for } \theta \in [0,\pi),$$

and perpendicular vectors

$$\mathbf{n}_\theta = \begin{bmatrix} \cos(\theta) \\ \sin(\theta) \end{bmatrix} \quad \text{and} \quad \mathbf{n}_\theta^\perp = \begin{bmatrix} -\sin(\theta) \\ \cos(\theta) \end{bmatrix},$$

where we let $\mathbf{x}_\theta = Q_\theta^{-1}\mathbf{x} = Q_\theta^T\mathbf{x}$, so that $\mathbf{x}_\theta = [\mathbf{x}^T\mathbf{n}_\theta, \mathbf{x}^T\mathbf{n}_\theta^\perp]^T \in \mathbb{R}^2$.

Note that any $\mathbf{y} \in \ell_{t,0}$ has the form $\mathbf{y} = [t, s]^T \in \mathbb{R}^2$ for parameter $s \in \mathbb{R}$. In the following, it will be convenient to let $\mathbf{v}_{t,s} := [t, s]^T = \mathbf{y}$ for $t, s \in \mathbb{R}$. This way, we obtain the representation

$$\begin{aligned} h_{t,\theta}(\mathbf{x}) &= \int_{\ell_{t,0}} \phi(\|\mathbf{x}_\theta - \mathbf{y}\|^2) w(\|\mathbf{y}\|^2)\,\mathrm{d}\mathbf{y} \\ &= \int_{\mathbb{R}} \phi(\|\mathbf{x}_\theta\|^2 - 2\mathbf{x}_\theta^T \mathbf{v}_{t,s} + \|\mathbf{v}_{t,s}\|^2) w(\|\mathbf{v}_{t,s}\|^2)\,\mathrm{d}s \\ &= \int_{\mathbb{R}} \phi(\|\mathbf{x}\|^2 - 2\mathbf{x}_\theta^T \mathbf{v}_{t,s} + \|\mathbf{v}_{t,s}\|^2) w(\|\mathbf{v}_{t,s}\|^2)\,\mathrm{d}s \\ &= \int_{\mathbb{R}} \phi\left((\mathbf{x}^T\mathbf{n}_\theta - t)^2 + (\mathbf{x}^T\mathbf{n}_\theta^\perp - s)^2\right) w(\|\mathbf{v}_{t,s}\|^2)\,\mathrm{d}s, \end{aligned} \tag{23}$$

where we have used the identity

$$\begin{aligned} &\|\mathbf{x}\|^2 - 2\mathbf{x}_\theta^T \mathbf{v}_{t,s} + \|\mathbf{v}_{t,s}\|^2 \\ &= \|\mathbf{x}\|^2 \pm (\mathbf{x}^T\mathbf{n}_\theta)^2 - 2\mathbf{x}^T\mathbf{n}_\theta t + t^2 \pm (\mathbf{x}^T\mathbf{n}_\theta^\perp)^2 - 2\mathbf{x}^T\mathbf{n}_\theta^\perp s + s^2 \\ &= \|\mathbf{x}\|^2 + \left(\mathbf{x}^T\mathbf{n}_\theta - t\right)^2 + \left(\mathbf{x}^T\mathbf{n}_\theta^\perp - s\right)^2 - \left[(\mathbf{x}^T\mathbf{n}_\theta)^2 + (\mathbf{x}^T\mathbf{n}_\theta^\perp)^2\right] \\ &= \left(\mathbf{x}^T\mathbf{n}_\theta - t\right)^2 + \left(\mathbf{x}^T\mathbf{n}_\theta^\perp - s\right)^2. \end{aligned}$$

Now we finally combine the representation for the weighted basis functions $g_{t,\theta}$ in (22) and that of their major part $h_{t,\theta}$ in (23). To this end, note that under the assumption $(\phi w)(|\cdot|^2) \in \mathrm{L}^1([0,\infty), \mathbb{R})$, the integral in (23) is finite for any $\mathbf{x} \in \mathbb{R}^2$. We conclude the discussion of this subsection as follows.

Proposition 3 *The weighted basis functions $g_{t,\theta} : \mathbb{R}^2 \to \mathbb{R}$ in (22) can be represented as*

$$g_{t,\theta}(\mathbf{x}) = \int_{\mathbb{R}} \phi\left((\mathbf{x}^T\mathbf{n}_\theta - t)^2 + (\mathbf{x}^T\mathbf{n}_\theta^\perp - s)^2\right) w(\|\mathbf{v}_{t,s}\|^2)\,\mathrm{d}s \cdot w(\|\mathbf{x}\|^2).$$

For $(\phi w)(|\cdot|^2) \in \mathrm{L}^1([0,\infty), \mathbb{R})$, $g_{t,\theta}(\mathbf{x})$ is for any $\mathbf{x} \in \mathbb{R}^2$ well-defined. □

3.2 Representation of the Matrix Entries

To solve the reconstruction problem

$$\mathcal{R}_\mathcal{L}(g) = \mathcal{R}_\mathcal{L}(f) \qquad \text{for } \mathcal{L} = \{\ell_1, \ldots, \ell_n\} \subset \mathbb{R}^2\,,$$

this requires solving the linear system (7) with matrix entries a_{kj} as in (21), i.e.,

$$a_{kj} = \mathcal{R}^{\mathbf{x}}_{\ell_j}\left[\mathcal{R}^{\mathbf{y}}_{\ell_k}\left[\phi(\|\mathbf{x} - \mathbf{y}\|^2) w(\|\mathbf{y}\|^2)\right] \cdot w(\|\mathbf{x}\|^2)\right]. \tag{24}$$

In our following computations, we let $\ell_k := \ell_{t,\theta}$ and $\ell_j := \ell_{r,\varphi}$ to indicate the dependence on the Radon lines' parameters $(t, \theta), (r, \varphi) \in \mathbb{R} \times [0, \pi)$.

Therefore, by using the representation of the weighted basis functions $g_{t,\theta}$ in Proposition 3, any matrix entry a_{kj} in (24) has the form

$$\begin{aligned} a_{kj} &= \mathcal{R}^{\mathbf{x}}_{\ell_{r,\varphi}}\left[g_{t,\theta}(\mathbf{x})\right] \\ &= \int_{\ell_{r,\varphi}} \left[\int_{\mathbb{R}} \phi\left((\mathbf{x}^T\mathbf{n}_\theta - t)^2 + (\mathbf{x}^T\mathbf{n}_\theta^\perp - s)^2\right) w(\|\mathbf{v}_{t,s}\|^2)\,\mathrm{d}s\right] w(\|\mathbf{x}\|^2)\,\mathrm{d}\mathbf{x}. \end{aligned} \tag{25}$$

Now the line integral of $g_{t,\theta}$ over $\ell_{r,\varphi}$ can be transformed into a line integral over $\ell_{r,0}$, so that we obtain for a_{kj} in (25) the representation

$$\begin{aligned} &\int_{\ell_{r,\varphi}} \left[\int_{\mathbb{R}} \phi\left((\mathbf{x}^T\mathbf{n}_\theta - t)^2 + (\mathbf{x}^T\mathbf{n}_\theta^\perp - s)^2\right) w(\|\mathbf{v}_{t,s}\|^2)\,\mathrm{d}s\right] w(\|\mathbf{x}\|^2)\,\mathrm{d}\mathbf{x} \\ &= \int_{\ell_{r,0}} \left[\int_{\mathbb{R}} \phi\left((\mathbf{x}^T Q_\varphi^T\mathbf{n}_\theta - t)^2 + (\mathbf{x}^T Q_\varphi^T\mathbf{n}_\theta^\perp - s)^2\right) w(\|\mathbf{v}_{t,s}\|^2)\,\mathrm{d}s\right] w(\|\mathbf{x}\|^2)\,\mathrm{d}\mathbf{x} \\ &= \int_{\ell_{r,0}} \left[\int_{\mathbb{R}} \phi\left((\mathbf{x}^T\mathbf{n}_{\theta-\varphi} - t)^2 + (\mathbf{x}^T\mathbf{n}_{\theta-\varphi}^\perp - s)^2\right) w(\|\mathbf{v}_{t,s}\|^2)\,\mathrm{d}s\right] w(\|\mathbf{x}\|^2)\,\mathrm{d}\mathbf{x} \\ &= \int_{\mathbb{R}} \left[\int_{\mathbb{R}} \phi\left((\mathbf{v}_{r,\tilde{s}}^T\mathbf{n}_{\theta-\varphi} - t)^2 + (\mathbf{v}_{r,\tilde{s}}^T\mathbf{n}_{\theta-\varphi}^\perp - s)^2\right) w(\|\mathbf{v}_{t,s}\|^2)\,\mathrm{d}s\right] w(\|\mathbf{v}_{r,\tilde{s}}\|^2)\,\mathrm{d}\tilde{s}, \end{aligned}$$

where we let $\mathbf{x} = (r,\tilde{s})^T = \mathbf{v}_{r,\tilde{s}}$.

Now, since

$$\begin{aligned} &(\mathbf{v}_{r,\tilde{s}}^T\mathbf{n}_{\theta-\varphi} - t)^2 + (\mathbf{v}_{r,\tilde{s}}^T\mathbf{n}_{\theta-\varphi}^\perp - s)^2 \\ &= (\mathbf{v}_{r,\tilde{s}}^T\mathbf{n}_{\theta-\varphi})^2 + (\mathbf{v}_{r,\tilde{s}}^T\mathbf{n}_{\theta-\varphi}^\perp)^2 - 2\mathbf{v}_{r,\tilde{s}}^T(\mathbf{n}_{\theta-\varphi}t + \mathbf{n}_{\theta-\varphi}^\perp s) + t^2 + s^2 \\ &= \|\mathbf{v}_{r,\tilde{s}}\|^2 - 2\mathbf{v}_{r,\tilde{s}}^T Q_{\theta-\varphi}\mathbf{v}_{t,s} + \|\mathbf{v}_{t,s}\|^2 \\ &= \|Q_\varphi\mathbf{v}_{r,\tilde{s}}\|^2 - 2(Q_\varphi\mathbf{v}_{r,\tilde{s}})^T(Q_\theta\mathbf{v}_{t,s}) + \|Q_\theta\mathbf{v}_{t,s}\|^2 \\ &= \|Q_\varphi\mathbf{v}_{r,\tilde{s}} - Q_\theta\mathbf{v}_{t,s}\|^2. \end{aligned} \tag{26}$$

Now we finally combine the representation for the matrix entries a_{kj} in (25) with that in (26). Note that under the assumption $(\phi w)(|\cdot|^2) \in \mathrm{L}^1([0,\infty),\mathbb{R})$, the double integral in the representation for a_{kj} in (25) is finite. We conclude the discussion of this subsection as follows.

Proposition 4 *Let $K_{\phi,w}(\mathbf{x},\mathbf{y})$ be a weighted kernel of the form* (15)*, where $(\phi w)(|\cdot|^2) \in \mathrm{L}^1(\mathbb{R})$. Then, all entries of the symmetric positive definite kernel matrix $A_{K,\mathcal{L}} = (a_{kj})_{1\le k,j\le n} \in \mathbb{R}^{n\times n}$ in* (19) *are well-defined, where the matrix entry a_{kj} in* (21) *is given as*

$$a_{kj} = \int_{\mathbb{R}}\int_{\mathbb{R}} \phi\left(\|Q_\varphi\mathbf{v}_{r,\tilde{s}} - Q_\theta\mathbf{v}_{t,s}\|^2\right) w(\|\mathbf{v}_{t,s}\|^2) w(\|\mathbf{v}_{r,\tilde{s}}\|^2)\,\mathrm{d}s\,\mathrm{d}\tilde{s}.$$

In particular, we have the representation

$$a_{kk} = \int_{\mathbb{R}}\int_{\mathbb{R}} \phi\left((\tilde{s}-s)^2\right) w(t^2+s^2) w(\tilde{s}^2+r^2)\,\mathrm{d}s\,\mathrm{d}\tilde{s}$$

for the diagonal entries of the matrix $A_{K,\mathcal{L}}$. □

4 Special Case: Gaussian Kernel and Gaussian Weight

In our numerical experiments, we considered using the special case, where $K_{\phi,w}(\mathbf{x},\mathbf{y})$ in (15) is given by a combination of the Gaussian kernel

$$\phi_\alpha(\|\mathbf{x}-\mathbf{y}\|^2) = \mathrm{e}^{-\alpha\|\mathbf{x}-\mathbf{y}\|^2} \qquad \text{for } \mathbf{x},\mathbf{y}\in\mathbb{R}^2 \text{ and } \alpha>0$$

and the Gaussian weight function

$$w_\beta(\|\mathbf{x}\|^2) = \mathrm{e}^{-\beta\|\mathbf{x}\|^2} \qquad \text{for } \mathbf{x}\in\mathbb{R}^2 \text{ and } \beta>0.$$

For the purposes of this paper, it is quite instructive to show how we computed the weighted Gaussian basis functions $g_{t,\theta}$ in Proposition 3 and the Gaussian matrix entries a_{kj} in Proposition 4 for this prototypical case. For other special cases, explicit representations for weighted basis functions $g_{t,\theta}$ and matrix entries a_{kj} should be elaborated by following along the lines of our following computations.

4.1 Weighted Gaussian Basis Functions

Starting from the representation of $g_{t,\theta}(\mathbf{x})$ in Proposition 3, we obtain

$$\begin{aligned}
&g_{t,\theta}(\mathbf{x})\\
&= \int_{\mathbb{R}} \mathrm{e}^{-\alpha\left[(\mathbf{x}^T\mathbf{n}_\theta - t)^2 + (\mathbf{x}^T\mathbf{n}_\theta^\perp - s)^2\right]}\, \mathrm{e}^{-\beta(t^2+s^2)}\,\mathrm{d}s \cdot \mathrm{e}^{-\beta\|x\|^2}\\
&= \mathrm{e}^{-\alpha\left[(\mathbf{x}^T\mathbf{n}_\theta - t)^2 + (\mathbf{x}^T\mathbf{n}_\theta^\perp)^2\right] - \beta(t^2+\|x\|^2)} \int_{\mathbb{R}} \mathrm{e}^{-\alpha\left[-2(\mathbf{x}^T\mathbf{n}_\theta^\perp)s + s^2\right] - \beta s^2}\,\mathrm{d}s\\
&= \mathrm{e}^{-\left[(\alpha+\beta)t^2 + \alpha\left((\mathbf{x}^T\mathbf{n}_\theta)^2 + (\mathbf{x}^T\mathbf{n}_\theta^\perp)^2 - 2(\mathbf{x}^T\mathbf{n}_\theta)t\right) + \beta\|x\|^2\right]} \int_{\mathbb{R}} \mathrm{e}^{-\left[(\alpha+\beta)s^2 - 2\alpha(\mathbf{x}^T\mathbf{n}_\theta^\perp)s\right]}\,\mathrm{d}s\\
&= \mathrm{e}^{-\left[(\alpha+\beta)(t^2+\|x\|^2) - 2\alpha(\mathbf{x}^T\mathbf{n}_\theta)t\right]} \int_{\mathbb{R}} \mathrm{e}^{-\left[(\alpha+\beta)s^2 - 2\alpha(\mathbf{x}^T\mathbf{n}_\theta^\perp)s \pm \frac{\alpha^2}{\alpha+\beta}(\mathbf{x}^T\mathbf{n}_\theta^\perp)^2\right]}\,\mathrm{d}s\\
&= \mathrm{e}^{-\left[(\alpha+\beta)(t^2+\|x\|^2) - 2\alpha(\mathbf{x}^T\mathbf{n}_\theta)t - \frac{\alpha^2}{\alpha+\beta}(\mathbf{x}^T\mathbf{n}_\theta^\perp)^2\right]} \int_{\mathbb{R}} \mathrm{e}^{-\left[\sqrt{\alpha+\beta}s - \frac{\alpha}{\sqrt{\alpha+\beta}}(\mathbf{x}^T\mathbf{n}_\theta^\perp)\right]^2}\,\mathrm{d}s,
\end{aligned}$$

so that we can draw the following conclusion.

Proposition 5 *For $(t,\theta)\in\mathbb{R}\times[0,\pi)$, the weighted Gaussian basis functions are given as*

$$g_{t,\theta}(\mathbf{x}) = \sqrt{\frac{\pi}{\alpha+\beta}} \cdot e^{-\left[(\alpha+\beta)(t^2+\|x\|^2) - 2\alpha(\mathbf{x}^T\mathbf{n}_\theta)t - \frac{\alpha^2}{\alpha+\beta}(\mathbf{x}^T\mathbf{n}_\theta^\perp)^2\right]} \qquad \textit{for } \mathbf{x}\in\mathbb{R}^2,$$

where $\alpha,\beta>0$. □

4.2 Gaussian Matrix Entries

To compute the entries a_{kj} of the Gaussian kernel matrix, we can rely on the following standard result from basic calculus.

Lemma 1 *For $c_0, c_1 \in \mathbb{R}$ and $c_2 > 0$, we have*

$$\int_{\mathbb{R}} \mathrm{e}^{-\left[c_0+c_1 s+c_2 s^2\right]} \,\mathrm{d}s = \sqrt{\frac{\pi}{c_2}}\, \mathrm{e}^{\frac{c_1^2}{4c_2}-c_0}.$$

Proof By completion of the square in the exponent of the integrand, we get

$$\int_{\mathbb{R}} \mathrm{e}^{-\left[c_0+c_1 s+c_2 s^2\right]} \,\mathrm{d}s = \int_{\mathbb{R}} \mathrm{e}^{-\left[c_0+\left(\frac{c_1}{2\sqrt{c_2}}+\sqrt{c_2}s\right)^2-\frac{c_1^2}{4c_2}\right]} \,\mathrm{d}s = \sqrt{\frac{\pi}{c_2}}\, \mathrm{e}^{\frac{c_1^2}{4c_2}-c_0},$$

where we have used the substitution $u = \frac{c_1}{2\sqrt{c_2}} + \sqrt{c_2}s$. □

Now we are in a position where we can compute the entries a_{kj} of the Gaussian matrix by using their representation in Proposition 4. To this end, we use similar calculations as in the outset of Section 3.2. We recall the representation $\mathbf{v}_{r,s} = (r,s)^T \in \mathbb{R}^2$ for a point on line $\ell_{r,0}$. Moreover, recall that for two perpendicular unit vectors $\mathbf{n}_\theta$ and $\mathbf{n}_\theta^\perp$ their rotation about angle $-\varphi$ is given by $Q_\varphi^T \mathbf{n}_\theta = \mathbf{n}_{\theta-\varphi}$ and $Q_\varphi^T \mathbf{n}_\theta^\perp = \mathbf{n}_{\theta-\varphi}^\perp$, respectively. This then yields

$$\begin{aligned} a_{kj} &= \int_{\ell_{r,\varphi}} \sqrt{\frac{\pi}{\alpha+\beta}} \mathrm{e}^{-\left[(\alpha+\beta)(t^2+\|\mathbf{x}\|^2)-2\alpha(\mathbf{x}^T\mathbf{n}_\theta)t-\frac{\alpha^2}{\alpha+\beta}(\mathbf{x}^T\mathbf{n}_\theta^\perp)^2\right]} \,\mathrm{d}\mathbf{x} \\ &= \sqrt{\frac{\pi}{\alpha+\beta}} \int_{\ell_{r,0}} \mathrm{e}^{-\left[(\alpha+\beta)(t^2+\|\mathbf{x}\|^2)-2\alpha((Q_\varphi\mathbf{x})^T\mathbf{n}_\theta)t-\frac{\alpha^2}{\alpha+\beta}((Q_\varphi\mathbf{x})^T\mathbf{n}_\theta^\perp)^2\right]} \,\mathrm{d}\mathbf{x} \\ &= \sqrt{\frac{\pi}{\alpha+\beta}} \int_{\mathbb{R}} \mathrm{e}^{-\left[(\alpha+\beta)(t^2+r^2+s^2)-2\alpha t(\mathbf{v}_{r,s}^T\mathbf{n}_{\theta-\varphi})-\frac{\alpha^2}{\alpha+\beta}(\mathbf{v}_{rs}^T\mathbf{n}_{\theta-\varphi}^\perp)^2\right]} \,\mathrm{d}s, \quad (27) \end{aligned}$$

With letting $\eta = \theta - \varphi$, and by using

$$\mathbf{v}_{r,s}^T\mathbf{n}_\eta = r\cos(\eta) + s\sin(\eta) \quad \text{and} \quad \mathbf{v}_{r,s}^T\mathbf{n}_\eta^\perp = s\cos(\eta) - r\sin(\eta),$$

we can rewrite the exponent in the integrand in (27) as

$$c_0 + c_1 s + c_2 s^2,$$

where we let

$$\begin{aligned} c_0 \equiv c_0(r,t,\eta) &= (\alpha+\beta)(r^2+t^2) - 2\alpha r t\cos(\eta) - \frac{\alpha^2}{\alpha+\beta} r^2\sin^2(\eta) \\ c_1 \equiv c_1(r,t,\eta) &= 2\alpha\sin(\eta)\left(\frac{\alpha}{\alpha+\beta} r\cos(\eta) - t\right) \\ c_2 \equiv c_2(\eta) &= \alpha+\beta-\frac{\alpha^2}{\alpha+\beta}\cos^2(\eta). \end{aligned}$$

Now note that c_2 is positive for any $\eta \in \mathbb{R}$,

$$c_2 = \alpha + \beta - \frac{\alpha^2}{\alpha+\beta}\cos^2(\eta) \geq \alpha + \beta - \frac{\alpha^2}{\alpha+\beta} = \frac{\beta(\beta+2\alpha)}{\alpha+\beta} > 0,$$

so that we can rely on Lemma 1 to obtain the representation

$$a_{kj} = \frac{\pi}{\sqrt{(\alpha+\beta)c_2}}\, \mathrm{e}^{\frac{c_1^2}{4c_2}-c_0}. \tag{28}$$

For the purpose of implementation, the following representation for the matrix entries is quite convenient.

Proposition 6 *The entries of the Gaussian matrix $A_{K,\mathcal{L}}$ in* (19) *are given as*

$$a_{kj} = \frac{\pi}{\sqrt{q_{\alpha,\beta}(\eta)}} \exp\left(-\beta(2\alpha+\beta)\cdot\frac{p_{\alpha,\beta}(t,r,\eta)}{q_{\alpha,\beta}(\eta)}\right), \tag{29}$$

where $\eta = \theta - \varphi$ and where

$$\begin{aligned} p_{\alpha,\beta}(t,r,\eta) &= (\alpha+\beta)(r^2+t^2) - 2\alpha rt\cos(\eta) \\ q_{\alpha,\beta}(\eta) &= (\alpha+\beta)^2 - \alpha^2\cos^2(\eta). \end{aligned}$$

Moreover, the matrix $A_{K,\mathcal{L}}$ is symmetric positive definite with diagonal entries

$$a_{kk} = \frac{\pi}{\sqrt{\beta(2\alpha+\beta)}}\, \mathrm{e}^{-2\beta t^2} > 0 \qquad \text{for any } (t,\theta) \in \mathbb{R}\times[0,\pi). \tag{30}$$

Proof Starting from the representation in (28), first note that

$$q_{\alpha,\beta}(\eta) = (\alpha+\beta)c_2.$$

Therefore, it remains to show the identity

$$\frac{c_1^2}{4c_2} - c_0 = -\beta(2\alpha+\beta)\cdot\frac{p_{\alpha,\beta}(t,r,\eta)}{q_{\alpha,\beta}(\eta)},$$

or, equivalently,

$$q_{\alpha,\beta}(\eta)\left(\frac{c_1^2}{4c_2} - c_0\right) = -\beta(2\alpha+\beta)\cdot p_{\alpha,\beta}(t,r,\eta). \tag{31}$$

To establish (31), we first represent the right hand side in (31) by

$$\begin{aligned} &-\beta(2\alpha+\beta)\cdot p_{\alpha,\beta}(t,r,\eta) \\ &= -\beta(2\alpha+\beta)\left[(\alpha+\beta)(r^2+t^2) - 2\alpha rt\cos(\eta)\right] \\ &= 2\alpha\beta(2\alpha+\beta)\cos(\eta)rt - \beta(2\alpha+\beta)(\alpha+\beta)(r^2+t^2). \end{aligned} \tag{32}$$

Now let us turn to the left hand side of (31). Note that

$$\begin{aligned}\frac{c_1^2}{4} &= \alpha^2 \sin^2(\eta) \left[\frac{\alpha^2}{(\alpha+\beta)^2} \cos^2(\eta) r^2 - 2\frac{\alpha}{\alpha+\beta} \cos(\eta) rt + t^2 \right] \\ &= \frac{\alpha^4}{(\alpha+\beta)^2} \cos^2(\eta)\sin^2(\eta) r^2 - 2\frac{\alpha^3}{\alpha+\beta} \cos(\eta)\sin^2(\eta) rt + \alpha^2 \sin^2(\eta) t^2.\end{aligned}$$

This in combination with $q_{\alpha,\beta}(\eta)/c_2 = \alpha + \beta$ yields

$$\frac{q_{\alpha,\beta}(\eta)}{c_2}\frac{c_1^2}{4} = \frac{\alpha^4 \cos^2(\eta)\sin^2(\eta)}{\alpha+\beta} r^2 - 2\alpha^3 \cos(\eta)\sin^2(\eta) rt + \alpha^2(\alpha+\beta)\sin^2(\eta) t^2.$$

Moreover, we find

$$\begin{aligned}&q_{\alpha,\beta}(\eta) \cdot c_0 \\ &= \left[(\alpha+\beta)^2 - \alpha^2\cos^2(\eta)\right] \left[(\alpha+\beta)(r^2+t^2) - 2\alpha\cos(\eta) rt - \frac{\alpha^2}{\alpha+\beta}\sin^2(\eta) r^2 \right] \\ &= (\alpha+\beta)^3(r^2+t^2) - 2\alpha(\alpha+\beta)^2\cos(\eta) rt - \alpha^2(\alpha+\beta)\sin^2(\eta) r^2 \\ &\quad - \alpha^2(\alpha+\beta)\cos^2(\eta)(r^2+t^2) + 2\alpha^3\cos^3(\eta) rt + \frac{\alpha^4}{\alpha+\beta}\cos^2(\eta)\sin^2(\eta) r^2 \\ &= \left[(\alpha+\beta)^3 - \alpha^2(\alpha+\beta) + \frac{\alpha^4}{\alpha+\beta}\cos^2(\eta)\sin^2(\eta) \right] r^2 \\ &\quad + 2\alpha\cos(\eta)\left[\alpha^2\cos^2(\eta) - (\alpha+\beta)^2\right] rt + \left[(\alpha+\beta)^3 - \alpha^2(\alpha+\beta)\cos^2(\eta)\right] t^2.\end{aligned}$$

This leads us to the representation

$$\begin{aligned}&q_{\alpha,\beta}(\eta) \cdot \left(\frac{c_1^2}{4c_2} - c_0 \right) \\ &= \left[\frac{\alpha^4}{\alpha+\beta}\cos^2(\eta)\sin^2(\eta) - (\alpha+\beta)^3 + \alpha^2(\alpha+\beta) - \frac{\alpha^4}{\alpha+\beta}\cos^2(\eta)\sin^2(\eta) \right] r^2 \\ &\quad + 2\alpha\cos(\eta)\left[(\alpha+\beta)^2 - \alpha^2\sin^2(\eta) - \alpha^2\cos^2(\eta)\right] rt \\ &\quad + \left[\alpha^2(\alpha+\beta)\sin^2(\eta) - (\alpha+\beta)^3 + \alpha^2(\alpha+\beta)\cos^2(\eta)\right] t^2 \\ &= \left[\alpha^2(\alpha+\beta) - (\alpha+\beta)^3\right](r^2+t^2) + 2\alpha\cos(\eta)\left[(\alpha+\beta)^2 - \alpha^2\right] rt \\ &= 2\alpha\beta(2\alpha+\beta)\cos(\eta) rt - \beta(2\alpha+\beta)(\alpha+\beta)(r^2+t^2)\end{aligned}$$

for the left hand side in (31), which coincides with the right hand side in (32).

The stated symmetry of the Gaussian matrix $A_{K,\mathcal{L}}$ is due to the symmetry of the functions $q_{\alpha,\beta}$ and $p_{\alpha,\beta}$ in (29), where we can in particular rely on

$$\begin{aligned} q_{\alpha,\beta}(\eta) &= q_{\alpha,\beta}(-\eta) \quad \text{for all } \eta \in \mathbb{R} \\ p_{\alpha,\beta}(t,r,\eta) &= p_{\alpha,\beta}(t,r,-\eta) \quad \text{for all } r,t,\eta \in \mathbb{R} \\ p_{\alpha,\beta}(t,r,\eta) &= p_{\alpha,\beta}(r,t,\eta) \quad \text{for all } r,t,\eta \in \mathbb{R}, \end{aligned}$$

so that, by using representation (29), we get

$$\begin{aligned} a_{kj} &= \frac{\pi}{\sqrt{q_{\alpha,\beta}(\eta)}} \exp\left(-\beta(2\alpha+\beta)\cdot\frac{p_{\alpha,\beta}(t,r,\eta)}{q_{\alpha,\beta}(\eta)}\right) \\ &= \frac{\pi}{\sqrt{q_{\alpha,\beta}(-\eta)}} \exp\left(-\beta(2\alpha+\beta)\cdot\frac{p_{\alpha,\beta}(r,t,-\eta)}{q_{\alpha,\beta}(-\eta)}\right) = a_{jk}. \end{aligned}$$

Let us finally turn to the diagonal entries a_{kk}. In this case, $\eta = \theta - \varphi = 0$ and $r = t$, so that due to

$$\begin{aligned} q_{\alpha,\beta}(0) &= \beta(2\alpha+1) \\ p_{\alpha,\beta}(t,t,0) &= 2\beta t^2. \end{aligned}$$

we obtain the stated representation (30). □

5 Numerical Examples

We have implemented the proposed kernel-based reconstruction scheme for the weighted Gaussian kernel

$$K_{\phi,w}(\mathbf{x},\mathbf{y}) = \phi_\alpha\left(\|\mathbf{x}-\mathbf{y}\|^2\right)\cdot w_\beta(\|\mathbf{x}\|^2)\cdot w_\beta(\|\mathbf{y}\|^2) \qquad \text{for } \alpha,\beta>0$$

by using the Gaussian kernel

$$\phi_\alpha(\|\mathbf{x}-\mathbf{y}\|^2) = \mathrm{e}^{-\alpha\|\mathbf{x}-\mathbf{y}\|^2} \qquad \text{for } \alpha>0$$

in combination with the Gaussian weight function

$$w_\beta(\|\mathbf{x}\|^2) = \mathrm{e}^{-\beta\|\mathbf{x}\|^2} \qquad \text{for } \beta>0.$$

For the purpose of illustration, we considered applying the proposed kernel-based reconstruction method to two popular phantoms:

(a) The phantom `bull's eye`, $f_{\mathrm{BE}} : [-1,1]^2 \to \mathbb{R}$, given as a linear combination

$$f_{\mathrm{BE}}(\mathbf{x}) = \chi_{B_{3/4}}(\mathbf{x}) - \frac{3}{4}\chi_{B_{1/2}}(\mathbf{x}) + \frac{1}{4}\chi_{B_{1/4}}(\mathbf{x}) \qquad \text{for } \mathbf{x}\in[-1,1]^2 \quad (33)$$

of three indicator functions χ_{B_r} on the disks (each centred at the origin $\mathbf{0}$)

$$B_r = \left\{\mathbf{x}\in\mathbb{R}^2 : \|\mathbf{x}\|\le r\right\} \qquad \text{for } r = 3/4, 1/2, 1/4.$$

The phantom bull's eye is shown in Figure 1 (top left).

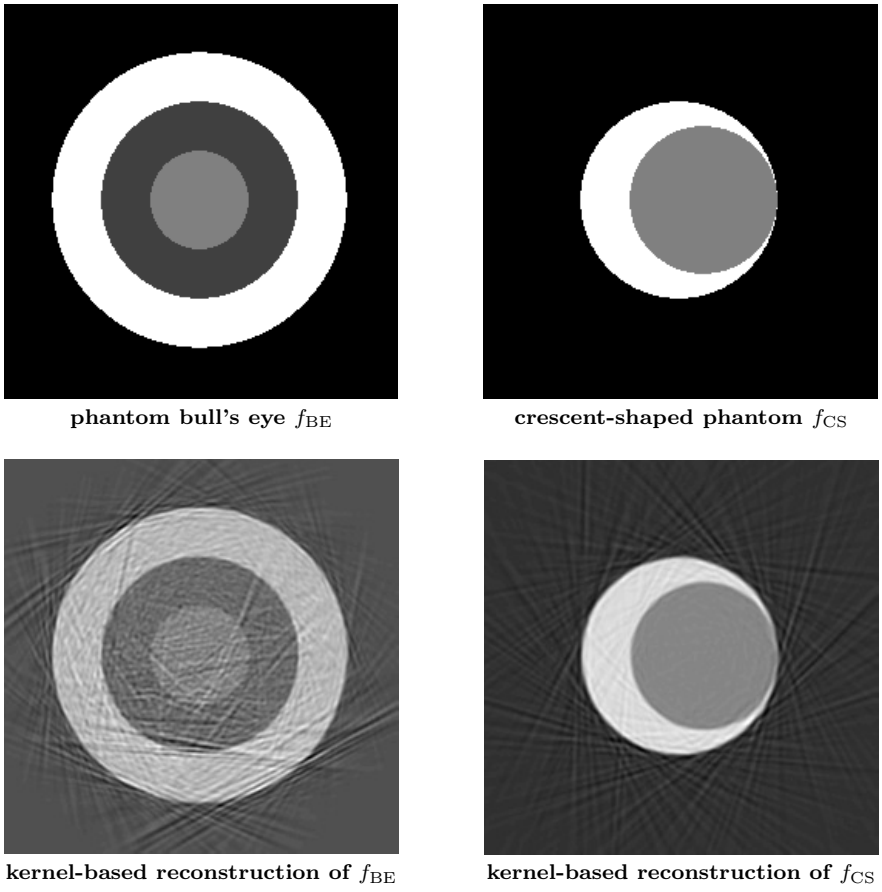

Fig. 1 Reconstruction of two phantoms by weighted Gaussian kernel functions. (a) `bull's eye`, as defined by f_{BE} in (33); (b) `crescent-shaped`, given as f_{CS} in (34). The reconstruction quality is further evaluated by MSE, PSNR, SSIM, cf. our results in Table 1.

(b) The `crescent-shaped` phantom $f_{\mathrm{CS}} : [-1,1]^2 \to \mathbb{R}$ is defined as

$$f_{\mathrm{CS}}(\mathbf{x}) = \chi_{B_{1/2}}(\mathbf{x}) - \frac{1}{2}\chi_{B_{3/8}(1/8,0)}(\mathbf{x}) \qquad \text{for } \mathbf{x} \in [-1,1]^2, \tag{34}$$

where

$$B_{3/8}(1/8,0) = \left\{\mathbf{x} = (x,y) \in \mathbb{R}^2 : (x-1/8)^2 + y^2 \le 9/64\right\}$$

is the disk of radius 3/8 centred at $(1/8, 0)$. The crescent-shaped phantom is shown in Figure 1 (top right). Note that f_{CS} is *not* radially symmetric, unlike f_{BE}.

In our numerical experiments we work with both *scattered* Radon data (see Subsection 5.1) and *regular* Radon data on parallel beam geometry (see

Subsection 5.2). Recall that for the case of scattered Radon data, standard Fourier-based reconstruction methods do not apply, as this is already explained in the introduction. Fourier-based FBP discretizations of the Radon transform usually rely on parallel beam geometry, see [5, Chapter 8]. Therefore, we have included numerical comparisons with FBP methods only in Subsection 5.2.

5.1 Reconstruction from Scattered Radon Data

For each test case, we acquired scattered Radon data $\{(\mathcal{R}f)(t_k,\theta_k)\}_{1\le k\le n}$ by line integrals of f over $n = 16,384$ scattered Radon lines $\{\ell_{t_k,\theta_k}\}_{1\le k\le n}$. To this end, we randomly chose line parameters $(t_k,\theta_k) \in [-\sqrt{2},\sqrt{2}] \times [0,\pi)$, for $1 \le k \le n$.

We measured the quality of our reconstruction g by the *mean square error*

$$\mathrm{MSE} = \frac{1}{J}\sum_{j=1}^{J}(f_j - g_j)^2,$$

where J is the size of the input image (i.e., the number of pixels), and where $f \equiv \{f_j\}_{j=1}^J$ and $g \equiv \{g_j\}_{j=1}^J$ are the greyscale values at the pixels of the target image f and of the reconstructed image g, respectively. In our numerical experiments, the image size is $J = 256 \times 256 = 65,536$. We remark that the MSE is by

$$\mathrm{PSNR} = 10 \times \log_{10}\left(\frac{(2^r-1)\times(2^r-1)}{\mathrm{MSE}}\right)$$

related to the *peak signal-to-noise ratio* (PSNR). In our numerical experiments, we have $r = 8$, giving the number of bits required for the representation of one luminance value.

Finally, we also recorded the *structural similarity index* (SSIM) to better measure the "similarity" between f and g. We remark that SSIM was designed in [16] to improve on the quality measures PSNR and MSE, particularly to obtain an enhanced consistency with human visual perception.

Our numerical results are shown in Figure 1 and in Table 1.

Table 1 Reconstruction of two phantoms by weighted Gaussian kernel functions.

phantom	α	β	MSE	PSNR	SSIM
bull's eye	7.0711	1.5166	0.0151	66.3314	0.3338
crescent-shaped	7.0711	1.0954	0.0054	70.8376	0.4752

We can conclude that the key features of the two test images are captured quite well by the proposed kernel-based reconstruction scheme. However, both their visual quality and their indicators MSE, PSNR, and SSIM may further be improved by fine-tuning the Gaussian shape parameters α and β. This,

however, is far beyond the aims of this paper, and therefore we decided to refrain from optimizing the method parameters α and β.

5.2 Reconstruction from Regular Radon Data on Parallel Beam Geometry

In this section, we assume that the input Radon data $(\mathcal{R}f)(t,\theta)$ are regular on *parallel beam geometry* (see [5, Section 8.4]). In this case, the angular variable $\theta \in [0,\pi)$ is discretized as

$$\theta_k = \frac{k\pi}{N} \qquad \text{for } k = 0,\ldots,N-1$$

for some $N \in \mathbb{N}$. Moreover, for each of the N angles θ_k, $k = 0,\ldots,N-1$, M Radon lines ℓ_{t_j,θ_k}, for $j = 1,\ldots,M$, are placed equispaced and parallel, such that they are orthogonal to the unit vector $\mathbf{n}_{\theta_k} = (\cos(\theta_k), \sin(\theta_k))$. This gives $N \times M$ Radon data $(\mathcal{R}f)(t_j,\theta_k)$. In our numerical experiments, we let $N = M = 128$, and $t_j \in [-\sqrt{2},\sqrt{2}]$, for $j = 1,\ldots,M$, i.e., the set of Radon data contains $N \times M = 16,384$ Radon lines.

We have applied the proposed kernel-based method to reconstruct the two phantoms f_{BE} in (33) and f_{CS} in (34). For comparison, we have also applied the Fourier-based filtered back projection (FBP) method. To this end, we considered using the Matlab function `iradon`, where we selected the option of *interpolation by linear splines* (for the back projection) in combination with the *Ram-Lak* low-pass filter. For details concerning the implementation of the FBP method we refer to [5].

Our numerical results are shown in Table 2 and in Figure 2, where the size of the output reconstructions is 90×90 each.

Table 2 Reconstruction of phantoms f_{BE} and f_{CS} on parallel beam geometry by kernel-based reconstruction versus Fourier-based reconstruction. The table shows the Gaussian shape parameters α, β of the kernel-based reconstruction, along with the resulting quality indicators PSNR(k) and SSIM(k). The quality indicators PSNR(f) and SSIM(f) of the Fourier-based method are shown for comparison. The obtained reconstructions of the phantoms f_{BE} and f_{CS} are displayed in Figure 2.

phantom	α	β	PSNR(k)	PSNR(f)	SSIM(k)	SSIM(f)
`bull's eye`	`6.8863`	`1.0613`	`54.3`	`54.1`	`0.452`	`0.447`
`crescent-shaped`	`7.0711`	`1.2397`	`58.0`	`57.9`	`0.730`	`0.726`

Given our numerical results, we can conclude that the proposed kernel-based reconstruction scheme is quite competitive. But we remark that the focus of this paper is on *scattered* data rather than on regular data.

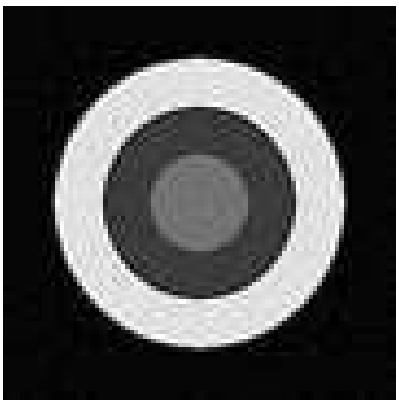

kernel-based reconstruction of f_{BE}

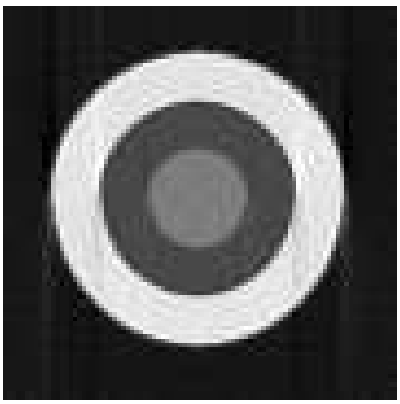

Fourier-based reconstruction of f_{BE}

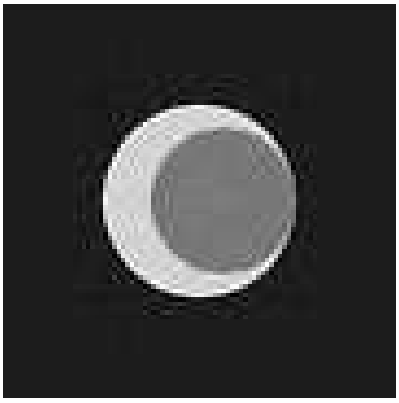

kernel-based reconstruction of f_{CS}

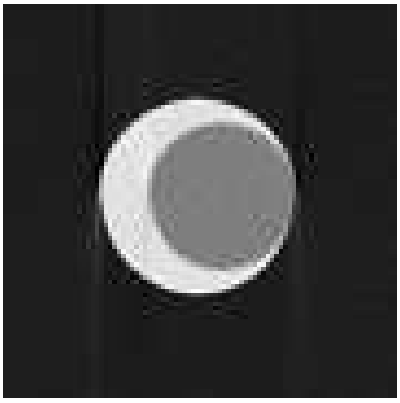

Fourier-based reconstruction of f_{CS}

Fig. 2 Reconstruction of phantoms f_{BE} and f_{CS} on parallel beam geometry. The reconstruction quality is further evaluated by PSNR and SSIM, cf. our results in Table 2.

References

1. R.K. Beatson and W. zu Castell: Scattered data interpolation of Radon data. Calcolo **48**, 2011, 5–19.
2. Å. Bjørck: *Numerical Methods for Least Squares Problems*. SIAM, Philadelphia, 1996.
3. S. Bochner: *Vorlesungen über Fouriersche Integrale*. Akademische Verlagsgesellschaft, Leipzig, 1932.
4. S. De Marchi, A. Iske, and A. Sironi: Kernel-based image reconstruction from scattered Radon data. Dolomites Research Notes on Approximation **9**, 2016, 19–31.
5. T.G. Feeman: *The Mathematics of Medical Imaging. A Beginner's Guide*. Second Edition, Springer Undergraduate Texts in Mathematics and Technology. Springer, New York, 2015.
6. R. Gordon, R. Bender, and G. Herman: Algebraic reconstruction techniques (ART) for three dimensional electron microscopy and X-ray photography. Journal of Theoretical Biology **29**(3), 1970, 471–481.
7. M. Guillemard and A. Iske: Interactions between kernels, frames, and persistent homology. In: *Recent Applications of Harmonic Analysis to Function Spaces, Differential Equations, and Data Science*. Volume 2: *Novel Methods in Harmonic Analysis*, I. Pesenson, Q.T. Le Gia, A. Mayeli, H. Mhaskar, and D.-X. Zhou (eds.), Birkhäuser, 2017, 861–888.

8. S. Helgason: *The Radon Transform*. Progress in Mathematics, vol. 5, 2nd edition. Birkhäuser, Basel, 1999.
9. A. Hertle: On the problem of well-posedness for the Radon transform. In: *Mathematical Aspects of Computerized Tomography*, G.T. Herman and F. Natterer (eds.), Lecture Notes in Medical Informatics, vol. 8, Springer, Berlin, 1981, 36–44.
10. A. Iske: *Charakterisierung bedingt positiv definiter Funktionen für multivariate Interpolationsmethoden mit radialen Basisfunktionen*. Dissertation, University of Göttingen,1994.
11. A. Iske: Reconstruction of functions from generalized Hermite-Birkhoff data. In: *Approximation Theory VIII, Vol. 1: Approximation and Interpolation*, C.K. Chui and L.L. Schumaker (eds.), World Scientific, Singapore, 1995, 257–264.
12. A. Iske: Scattered data approximation by positive definite kernel functions. Rend. Sem. Mat. Univ. Pol. Torino **69**(3), 2011, 217–246.
13. F. Natterer: *The Mathematics of Computerized Tomography*. Classics in Applied Mathematics, vol. 32. SIAM, Philadelphia, 2001.
14. J. Radon: Über die Bestimmung von Funktionen durch ihre Integralwerte längs gewisser Mannigfaltigkeiten. Berichte Sächsische Akademie der Wissenschaften **69**, 1917, 262–277.
15. R. Schaback and H. Wendland: Characterization and construction of radial basis functions. *Multivariate Approximation and Applications*, N. Dyn, D. Leviatan, D. Levin, and A. Pinkus (eds.), Cambridge University Press, Cambridge, 2001, 1–24.
16. Z. Wang, A.C. Bovik, H.R. Sheikh, and E.P. Simoncelli: Image quality assessment: from error visibility to structural similarity. IEEE Transactions on Image Processing **13**(4), April 2004, 600–612.
17. H. Wendland: *Scattered Data Approximation*. Cambridge University Press, 2005.

Acknowledgement. The authors thank one anonymous referee for suggesting an improvement concerning Proposition 1. The first author was supported by the project *"Multivariate approximation with application to image reconstruction"* of the University of Padova, years 2013-2014. The third author thanks the German Research Foundation (DFG) for financial support within the *Cluster of Excellence in Simulation Technology* (EXC 310/2) at the University of Stuttgart. The research of the first and the third author has been accomplished within RITA (Rete ITaliana di Approssimazione).